Letters in Applied NanoBioScience
Open-Access Journal (ISSN: 2284-6808)

Article
Volume 15, Issue 1, 2026, 46
https://doi.org/10.33263/LIANBS151.046

In silico Modeling for Dual Inhibition of Dipeptidyl Peptidase-4 and Xanthine Oxidase in Diabetes Mellitus

Sneha Tidke [1], Sapan K Shah [1,*], Dinesh Chaple [1]

[1] Department of Pharmaceutical Chemistry, Priyadarshini J. L. College of Pharmacy, Hingna Road, Nagpur-440016, Maharashtra, India
* Correspondence: shah.sapan@rediffmail.com;

Received: 20.08.2024; Accepted: 24.02.2026; Published: 30.03.2026

Abstract: In the present work, 215 and 35 compounds of dipeptidyl peptidase-4 (DPP-4) and xanthine oxidase (XO) inhibitors were selected from the ChEMBL database previously reported with potent anti-diabetic activity to develop GA-MLR-based QSAR models to identify the structural features that significantly correlate with the biological response. GA-MLR models went through rigorous validation using OECD principles. ADME and toxicity screening were performed for 50 newly designed molecules. The QSAR model aims to provide insights into dual inhibitory activities and their correlation with ligand-receptor interaction, crucial for designing safer dual inhibitors for diabetes management and identifying important descriptors and their structural features. The developed QSAR models are statistically robust (R^2 = 0.68-0.89) and have substantial external predictive performance (CCC_{ex} = 0.80-0.84). Compounds 08, 09, and 10 are docked according to RMSD, ADME, and toxicity rules, and are predicted to have higher pIC50 and experimental docking scores than standard drugs such as Sitagliptin and Allopurinol. QSAR analysis and docking results revealed that compound no. 08, 09, and 10 are showing better results than standard drugs by considering pIC_{50} and docking score. These compounds might be useful drug candidates for the treatment of diabetes and its related complications.

Keywords: QSAR; dipeptidyl peptidase-4; xanthine oxidase; molecular docking; anti-diabetic; genetic algorithm.

1. Introduction

Over 30 million Americans currently have diabetes, making it a fairly widespread condition in this country. 9.4% of the nation's citizens are represented by this. In the United States, diabetes is the seventh most common cause of mortality. High blood glucose levels at fasting times are a defining feature of diabetes mellitus. After the patient has fasted without eating anything throughout the previous night, a blood sample is taken to test this [1]. There are two main types of diabetes, type 1 and type 2, which are distinct from one another. In people with type 1, the pancreatic beta (ß) cells are no longer able to release insulin. Blood glucose levels rise, leading to a condition known as hyperglycemia. People under the age of 18 are diagnosed with type 1 diabetes in over 75% of instances. When the pancreatic beta cells can no longer allow glucose to enter to make energy, type 2 diabetes develops. According to studies, those who are overweight or obese, inactive, and have a family history of type 2 diabetes are more likely to get the disease [2]. Even though diabetes has been around far longer

than in the 1980s, it is now better understood. The idea is that the elements of the contemporary diet and lifestyle are connected to a "newer" disease. Diabetes mellitus has been linked to increased calorie intake, inadequate physical exercise, and obesity, which is now much more prevalent than it used to be. This circumstance happens everywhere. Diabetes has been documented in writing for thousands of years across various nations [3]. Diabetes mellitus is a serious condition that affects a huge portion of the population. This is a set of metabolic disorders characterized by poor metabolism of carbohydrates, proteins, and lipids. The most defining cause of insulin resistance or insufficient pancreatic release of insulin is hyperglycemia, which can result from either a hereditary or acquired abnormality in the pancreas [4]. In the Western world, diabetes mellitus is a major source of morbidity. Due to insulin insensitivity, a crucial hormone in glucose metabolism, this condition is characterized by excessive blood glucose levels [5]. One crucial early indicator of renal deterioration in diabetic patients is the kidneys' failure to stop urine protein leakage [6]. Chronic diabetes mellitus develops when the body is unable to manufacture enough insulin or use it efficiently [7]. Its main characteristic is persistent hypertension with vascular problems that can result in blindness, infection, brain damage, heart malfunction, and other issues [8]. DPP-4 is a serine exopeptidase that is widely distributed in the body and cleaves a variety of substrates, including glucose-dependent insulinotropic polypeptide (GIP) and glucagon-like peptide 1 (GLP-1), which are crucial for glucose regulation by stimulating insulin release in a glucose-dependent manner [9,10]. Therefore, DPP-4 inhibitors represent a relatively new class of oral glucose-lowering medications with good efficacy in treating type 2 diabetes [11]. Clinical findings also indicate that they may lessen albuminuria in type 2 diabetes patients [12]. Independent of islet-cell antibody status, C-peptide concentration, disease duration, or glycated hemoglobin (HbA1c), recent studies show that DPP-4 activity is higher in patients with T1DM than in healthy controls, even compared with type 2 DM [13]. It is widely expressed in most tissues, including lymphocytes, the placenta, uterus, prostate, gastrointestinal tract, and liver [14]. Four DPP-4 inhibitors have received FDA approval in the US: sitagliptin, saxagliptin, linagliptin, and alogliptin. This family of drugs has a good profile in that it has a low risk of hypoglycemia and is weight-neutral. Previous prospective randomized controlled trials have assessed the CV safety of sitagliptin, saxagliptin, and alogliptin (RCTs). Lately, the findings of 2 new trials assessing the CV safety of linagliptin were reported [15]. Nasopharyngitis, headaches, upper respiratory tract infections, and, less frequently and arguable, pancreatitis are known side effects of DPP4 inhibitors. Bullous pemphigoid is one of the recent reports of adverse medication reactions that are skin-related [16]. Hypoxanthine/xanthine is converted to uric acid by the enzyme XO in a process that also releases superoxide. The relationship between elevated uric acid levels, or hyperuricemia, and diabetes mellitus has been hotly debated because some studies claim it is a side effect of the disease, while others claim it is a risk factor for the onset of type 2 diabetes mellitus (T2DM) [17]. In the pathophysiology of many diseases, including gout, heart failure, stroke, atherosclerosis, diabetes, hypertension, colitis, inflammatory bowel diseases, and rheumatoid arthritis, excessive reactive oxygen species (ROS) and uric acid are generated by Xanthine Oxidase. One of the best treatments for renal dysfunctions linked to gout and hyperuricemia is XO inhibition [18,19]. A growing body of research indicates that inhibiting XO offers numerous therapeutic benefits for treating disorders like gout as well as cardiovascular problems, neural malfunction, aging, etc. One of the well-known XO inhibitors (XOIs) in clinical use is allopurinol; however, it has several side effects, such as hypersensitivity syndrome. This prompts researchers to seek novel, inexpensive XOIs with

minimal side effects to treat a variety of illnesses in which inflammation and free radicals play a significant pathophysiological role [20]. The production of xanthine and hypoxanthine was demonstrated to be effectively suppressed by ADA inhibition. Sitagliptin, a DPP-4 inhibitor, was demonstrated to raise interstitial adenosine levels, decrease XO substrates and uric acid levels, and mitigate oxidative stress in non-diabetic infarcted rats. The beneficial effects of sitagliptin were comparable to those of an ADA inhibitor and were countered by exogenous hypoxanthine and adenosine A1 receptor antagonists. Endogenous adenosine has a variety of functions, including endothelial protection, the reduction of reactive oxygen species (ROS) release, and protection of the ischemic myocardium [21,22]. In previous studies, a small dataset of DPP-4 and XO compounds was used for individual modeling, while in this work, a large dataset of DPP-4 and XO inhibitors was used [23–26].

Computational methods significantly contribute to drug discovery by employing multiple steps, including data collection, pre-processing, analysis, and evaluation. Fundamental concepts of molecular modelling and virtual experimentation reduce the need for wet-lab chemical experiments and are increasingly used to design multitargeted drugs for chronic diseases [27,28]. Quantitative Structure-Activity Relationships (QSAR) and Quantitative Structure-Property Relationships (QSPR) are two types of structure-activity relationship studies. These investigations seek to establish and quantify the connection between molecular structure and biological activity or property. The QSAR field may be regarded as the very first computer-aided method of drug discovery. Since the introduction of the idea, numerous QSAR approaches have been developed [29]. The popularity of QSAR has led researchers, particularly in the pharmaceutical industry, to develop a variety of QSAR methodologies. Using in-silico mathematical modeling approaches, Sapre *et al*. recently created 18 novel NNRTIs with high efficacy, and the outcomes were verified using the docking technique [30]. These comprise preparing the dataset, selecting and creating molecular descriptors, developing mathematical or statistical models, training and validating the models using training datasets, and testing the models using testing datasets [31]. Descriptors are the numerical representations of molecules used to perform the mathematical correlation of chemical structures with biological activities. They are the following: Averaged (dependent) descriptors, Electrostatic descriptors, Molecular-orbital-related descriptors, Constitutional descriptors [32], Topological descriptors [33], Geometrical descriptors, Electrostatic descriptors, Quantum chemical descriptors, and physicochemical descriptors [34]. We can characterize how small molecules bind to target proteins and shed light on basic biological processes by using molecular docking to model their interactions at the atomic level. Prediction of the ligand structure, as well as its placement and orientation within these sites, and evaluation of the binding affinity, are the two fundamental processes in the docking process [35]. At the moment, molecular docking is a common computational approach in drug design for lead compound optimization and virtual screening studies to uncover new physiologically active compounds. Because of its therapeutic uses in contemporary structure-based drug design, "protein-ligand docking" is recognized as a significant form of molecular docking [36]. Two key prerequisites for molecular docking are methods to predict protein-ligand poses and binding energies, as well as 3D structural data for the proposed ligand and the protein target of interest [37].

A comprehensive range of statistical, chemical, and computational methods is used in a QSAR analysis to develop and test a mathematical model that accounts for the association between desired activities and structural properties. The following are the main steps in a QSAR analysis [38–40]. Structure drawing and optimization (a) and interpretation of the

molecular descriptor computation (b). These processes combine concepts, tools, algorithms, and approaches from numerous scientific disciplines, including computing, mathematics, statistics, and others. As a result, the appropriately validated and deciphered QSAR analysis that was produced could be helpful in two different ways: (a) to predict a molecule's activity before its actual synthesis and bio-screening (Quantitative/Predictive QSAR), and (b) to identify the structural features/patterns that regulate the biological profile for a series of congeneric molecules [41].

From the literature review, a QSAR model for diabetes mellitus was developed, focusing on xanthine oxidase and dipeptidyl peptidase-4 as individual targets. Although both enzymes were investigated together, no model for their dual inhibition was created. Therefore, we aimed to develop a QSAR model that addresses the simultaneous inhibition of both DPP-4 and XO in the treatment of diabetes mellitus.

2. Materials and Methods

2.1. Experimental dataset.

In the present work, dipeptidyl peptidase-4 and xanthine oxidase inhibitors' activities were taken into consideration. The database was selected from the ChEMBL database for dipeptidyl peptidase 4 and xanthine oxidase, containing 215 and 35 compounds, respectively, as enzyme inhibitors, and was subjected to QSAR modeling. Smile notations are copied in Excel format. Announced estimations of IC_{50} (mol/L) were changed over to pIC_{50} by taking a negative logarithm ($pIC_{50} = -\log_{10}IC_{50}$) and thereafter used as the dependent variable for the 2D-QSAR model development [42].

2.2. Structure drawing and optimization.

In the current work, the QSAR examination observed the OECD guideline (https://www.oecd.org/en/publications/guidance-document-on-the-validation-of-quantitative-structure-activity-relationship-q-sar-models_9789264085442-en.html). The synthetic designs were drawn utilizing OpenBabel free software, followed by energy minimization using the MMFF94 force field [43]. The enhanced constructions were utilized as a contribution to the estimation of a decent number of 2D descriptors. For descriptor estimation, OCHEM online software (https://ochem.eu) was used for Pydescriptor calculation [44].

2.3. Molecular descriptor calculation.

Molecular descriptors are the transformations of one or more characteristics of the molecular structure into a set of numeric values, obtained using an unambiguous algorithm. In this work, 16383 molecular descriptors of dipeptidyl peptidase-4 (supplementary data 1) and 16380 molecular descriptors of xanthine oxidase (supplementary data 2), a total of 32763 molecular descriptors were calculated using Ochem online software [45]. Nearly constant (>95%) descriptors eliminated leads to 9980 descriptors of DPP-4 (supplementary data 3) and 9064 descriptors of XO (supplementary data 4) and highly correlated ($|R| > 95\%$) descriptors were also eliminated which leads to 976 (supplementary data 5) and 426 (supplementary data 6) descriptors of dpp4 and XO, using QSARINS [46].

2.4. Model development.

The Genetic Algorithm (GA) module found in QSARINS-2.2.1 was used to perform the subjective feature selection (SFS), which involved choosing the ideal number and set of molecular descriptors to use in the final models. The default settings were used, with the exception that the number of generations was set to 10,000. The dataset was divided into a training set (70%) and a prediction set (30%) for the model-building process. DPP-4 has 152 training compounds and 63 prediction compounds, and for xanthine oxidase, 26 training compounds and 9 prediction compounds. The final model was created by selecting the appropriate molecular descriptors from the training set. Only the final QSAR model was validated using the prediction set. It results in 337 descriptors of DPP-4 and 76 descriptors of XO after further correlated descriptors are eliminated. The final model was selected to guarantee a balance of qualitative and quantitative QSAR model characteristics, specifically simplicity, understandable molecular descriptors, accuracy, and extensive internal and external validation. Figure 1 shows the model development strategy that was employed.

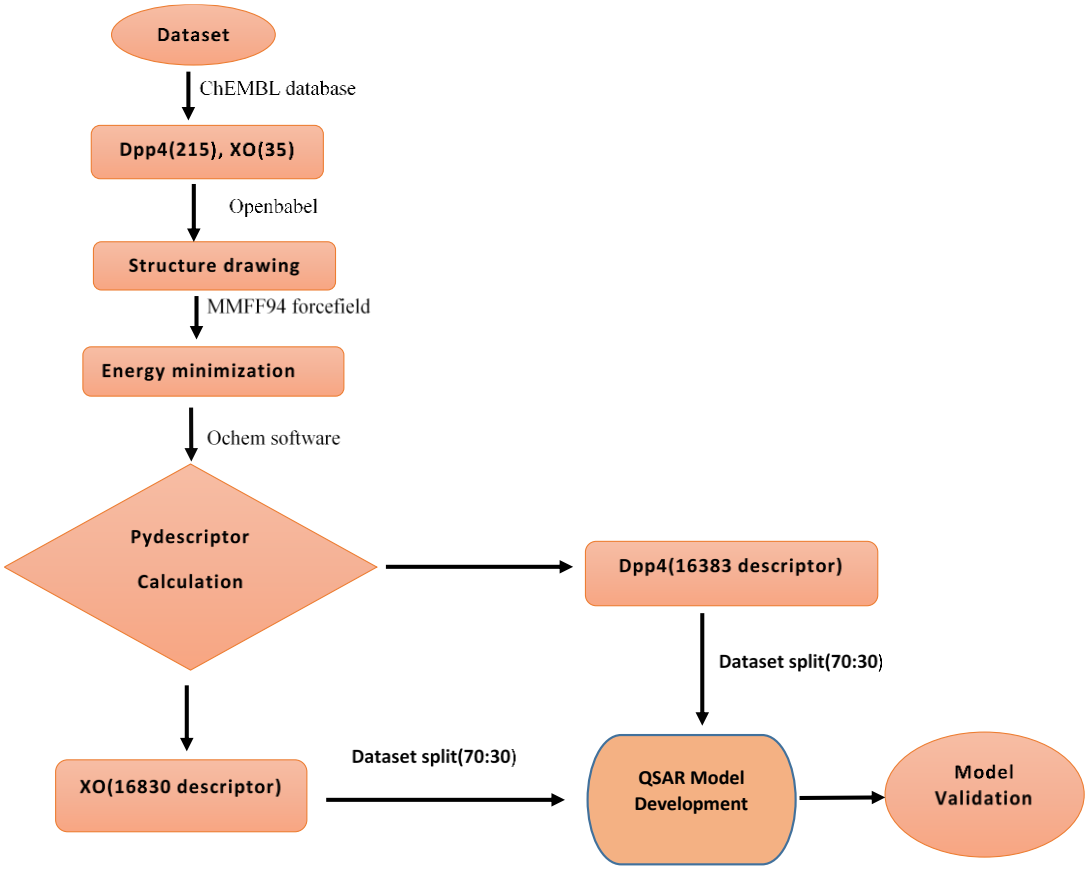

Figure 1. A strategy used for the QSAR model development.

2.5. Model validation.

All QSAR models must be properly verified to determine their utility and predictive power. The prediction set, data randomization (i.e., Y-scrambling), internal validation or cross-validation (CV) by leave-one-out (LOO) and leave-many-out (LMO) procedures, and (d) determining whether the following conditions are met were used to establish the statistical qualities and validity of the QSAR models. With $RMSE_{tr}$ $RMSE_{cv}$, CCC 0.80 with RMSE and MAE near zero, $R^2_{tr} > 0.6$, $Q^2_{loo} > 0.5$, $Q^2_{LMO} > 0.6$, $R^2_{ex} > 0.6$, and CCC > 0.80. The GA-MLR (Multi-linear Regression) model's robustness and high external predictability are confirmed by

the threshold values of these parameters. As a result, all models with poor internal and external prediction capacities were later eliminated [47].

2.6. Designing a new molecule.

Compounds of DPP-4 and XO are sorted out based on IC_{50} (< 600 nm) values as active and inactive compounds (supplementary data 7). The 15 reported compounds showing dual inhibitory activity were considered, and their py-descriptor values were calculated (supplementary data 8) [48]. Active compounds of DPP-4 and XO compared with the reported 15 compounds based on optimum descriptor values (supplementary data 9). Compound number 05 was selected as an ideal for designing new molecules, as its XO descriptor values are optimal, and a few DPP-4 descriptors' values need to be modified. Therefore, compound 05 was selected as a model for designing a new molecule using the Topliss scheme, the Bioisostere method, and randomly selected compounds. A total of 50 molecules were designed, their py-descriptor calculated, and the pIC_{50} value estimated using the model equation (supplementary data 10). These design molecules of DPP-4 and XO are used for molecular docking (Figure 2).

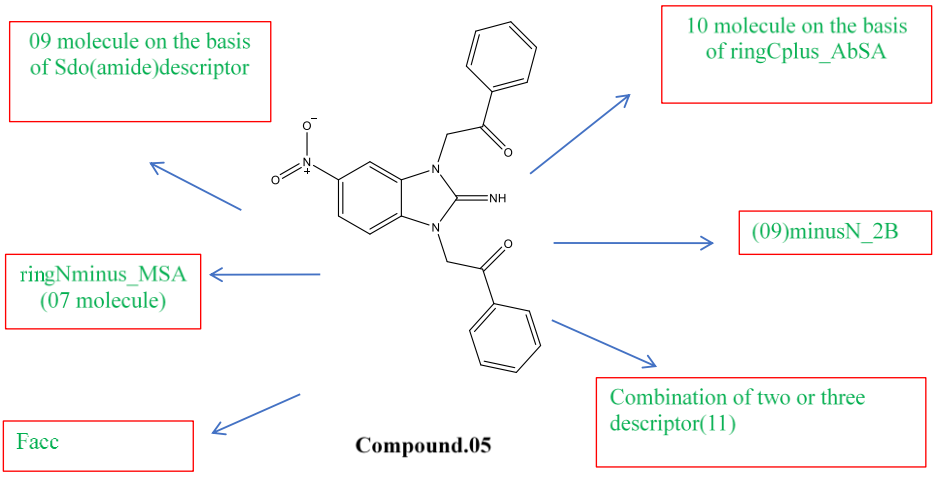

Figure 2. A total of 50 molecules were designed based on the Topliss scheme, and in the Bioisostere method, some molecules were designed randomly by considering compound 05 as ideal.

2.7. Molecular docking.

The X-ray crystal structures of DPP-4 (PDB ID: 4A5S) and XO (PDB ID: 3NVY) were chosen, and geometry optimization was carried out in PyRx using OpenBabel's UFF force field, which was used as the default dynamics parameter. Chain A should be chosen, all crystallization water eliminated, and the file should be saved in pdbqt format for future molecular docking [49]. The grid box for molecular docking was defined around the active sites of the target proteins based on their co-crystallized ligands. For DPP-4 (PDB ID: 4A5S), the grid box size was set to 25 × 25 × 25 Å, centered at coordinates 14.136 (x), 35.866 (y), and 54.839 (z). Similarly, for XO (PDB ID: 3NYV), the grid box dimensions were 25 × 30 × 25 Å, with the center located at 36.363 (x), –5.975 (y), and 24.171 (z). These grid settings ensured optimal coverage of the binding pockets for accurate ligand docking.

2.8. ADME screening.

ADME screening was done for 50 design molecules and sorted out for Lipinski rule, Ghose violation, Egan violation, Veber violation, and Muegg violation, which gives 27

compounds. All 27 compounds obey the rules; the rest are not considered for further screening. Then these 27 compounds are sorted out based on pIC_{50} having above 06, which leads to 17 compounds [50,51].

2.9. Toxicity screening.

A total of 17 compounds were screened for the prediction of toxicity using the ProTox-II web tool [52]. Out of 17 compounds, only 03 compounds obey the rule of inactive profile for hepatotoxicity, mutagenicity, carcinogenicity, immunogenicity, and another parameter [44]. As other compounds have active profiles related to toxicity, we finalized compound no. 08, 09, and 10.

3. Results and Discussion

3.1. QSAR model.

The major goal of the current effort is to find significant descriptors and to explain and understand them in terms of structural aspects. Therefore, QSAR models were created using random splitting (Table 1). The GA-MLR model has strong predictive ability and uses simple molecular descriptors to provide a clear interpretation of structural properties. The creation of a strong MLR model was the outcome of the GA study. Based on its statistical performance, the QSAR model will choose the MLR model (Table 2) [53].

Table 1. Developed and selected the best QSAR models.

Model 1	pIC_{50}=	-0.1549(±0.0988)SaasC - 0.1661(±0.0295)SdO(amid) + 0.0470(±0.0154)ringCplus_AbSA - 0.0326(±0.0172)ringNminus_MSA + 0.2704(±0.0750)minus_N_2B +0.1369(±0.0988)faccC3B + 6.3090
	Fitting criteria: N_{tr}=152, N_{test}=63, R^2=0.6832, Q^2loo=0.6509, CCC ext=0.8042	
Model 2	pIC_{50}=	-13.5800(±4.6099) fmsaminus-0.1243(±0.0608) + nCpcplus+0.0127(±0.0080) lipo_AbSA-3.8674(±2.0877)N_ringC_5Ac + 7.4751(±1.6718) C_ringN_6Bc + 11.1313
	Fitting criteria: N_{tr}=26, N_{test}=09, R^2=0.8901, Q^2loo=0.8311, CCC ext=0.8476	

3.1.1. Descriptor interpretation.

QSAR analysis is briefly described below, including the descriptors used in models.

ringCplus_AbSA: The molecular descriptor ringCplus_AbSA is a geometric descriptor representing the absolute surface area of a positively charged ring of a carbon atom. This descriptor has a positive coefficient; henceforth, its value must be as high as possible. To achieve this goal, the number of atoms needs to be increased around the aromatic ring to increase the activity.

minus_N_2B: It is a topological descriptor that represents the number of the negatively charged atom from nitrogen within 2 bonds, and it also has a positive correlation within 2 bonds of the negatively charged atom from nitrogen. Hence, its value needs to be increased within 2 bonds to achieve this goal or to increase the activity.

faccC3B: faccC3B is a circular fingerprint type of descriptor representing the frequency of occurrence of an acceptor atom from a carbon atom within 3 bonds. Has a positive coefficient, where an increase in the acceptor atom from the carbon atom within 3 bonds could lead to a better affinity for the target enzyme.

SaasC and ringNminus_MSA: SaasC molecular descriptor represents the sum of E-state values of the aromatic Carbon atom bound to known hydrogen, and

ringNminus_MSA represents the molecular surface area of the negatively charged ring N-atom. Both have negative coefficients; they should be as low as possible.

lipo_AbSA: This molecular descriptor is a geometric type descriptor and represents the absolute surface area of the lipophilic group. A positive coefficient increase in a lipophilic group will lead to enhanced activity in the present work.

C_ringN_6Bc: It represents the sum of partial charges of the carbon atom present within 6 bonds from the ring nitrogen atom, which also has a positive coefficient. An increase in rings containing nitrogen atoms increases the activity.

SdO(amid): Represents the sum of the E-state index of doubly bonded oxygen of amide, which has a negative coefficient in the model, so a decrease in double bond oxygen of amide in the structure will help to enhance the activity.

Fmsaminus and nCpcplus, and N_ringC_5Ac: In model 2 Fmsaminus represent frequency of occurrence of negatively charged surface area where nCpcplus represent number of C atoms having positive partial charges and N_ringC_5Ac represent sum of partial charge of nitrogen atom within 5 A° from ring carbon atom, all these three descriptors are having negative coefficient with the model so decrease in their value promote the activity in present work.

R^2 (correlation coefficient) values for models 1 and 2 are 0.6832 and 0.8901 (Table 2). Models 1 and 2 have concordance correlation coefficients of 0.8118 and 0.9418, respectively, and both models' Q^2_{loo} values are higher than 0.6. For both models, R^2_{ext} and CCC_{ext} are over 0.6. Since all statistical parameter values fall under the cut-off range, the model demonstrates this. The model's robustness and strong capacity to forecast the outside world are confirmed by the threshold values of these parameters. The statistical symbols have their typical meanings, which are referred to from literature [54–56]. The created QSAR models are statistically robust and have strong external prediction power, notably Model 2, as shown by statistical analysis. The created models' R^2_{adj}. Value is pretty close to R^2_{tr}, indicating that the number of descriptors in the models is not excessive and that over-fitting is not a problem [57].

Table 2. Statistical performance of the QSAR models.

Sr.No.	Statistical parameter	Model 1	Model 2
	Fitting Criteria		
01	R^2	0.6832	0.8901
02	R^2_{adj}	0.6701	0.8626
03	R^2-R^2_{adj}	0.0131	0.0275
04	LOF	0.7770	0.3835
05	Kxx	0.4213	0.4842
06	Delta K	0.220	0.0485
07	$RMSE_{tr}$	0.8119	0.3811
08	MAE_{tr}	0.6336	0.2889
09	RSS_{tr}	100.194	3.7760
10	CCC_{tr}	0.8118	0.9418
11	S	0.8313	0.4345
12	F	52.1290	32.3886
	Internal Validation Criteria		
01	Q^2_{loo}	0.6509	0.8311
02	R^2-Q^2_{loo}	0.0323	0.0590
03	$RMSE_{cv}$	0.8523	0.4724
04	MAE cv	0.6649	0.3665
05	$PRESS_{cv}$	110.4264	5.8016
06	CCC_{cv}	0.7928	0.9120
07	Q^2_{LMO}	0.6428	0.7990
08	R^2_{Yscr}	0.0393	0.1940
09	Q^2_{Yscr}	-0.0565	-0.4423

Sr.No.	Statistical parameter	Model 1	Model 2
10	RMSE AV_{Yscr}	1.4138	1.0296
External Validation Criteria			
01	$RMSE_{ext}$	0.7525	0.2837
02	MAE_{ext}	0.5380	0.2152
03	$PRESS_{ext}$	35.6754	0.7401
04	R^2_{ext}	0.6543	0.7401
05	Q^2-$_{F1}$	0.6394	0.8265
06	Q^2-$_{F2}$	0.6327	0.6339
07	Q^2-$_{F3}$	0.7279	0.9391
08	CCC_{ext}	0.8042	0.8476
09	r^2_m aver	0.5298	0.6176
10	r^2_m delta	0.0736	0.2261

R^2-correlation coefficient; Q^2-leave-one-out 'cross-validated R^2'; R^2-adjusted; SEE- standard error of estimates; RMSE - root mean squared error; MAE - mean absolute error; CCC - concordance correlation coefficient for the training (tr); and test (ex) sets; LOF - lack of fit, F Fischer's value; R^2_{LMO} and Q^2_{LMO} - leave many-out correlation coefficient and cross-validation coefficients; R^2_{Yscr} and Q^2_{Yscr} -scramble correlation and cross-validation coefficient.

The fact that both models' LOF (Lack of Fit) values are low further supports this. All of the models' low Kxx values, which represent the intercorrelation of the descriptors, show that there is little connection between the descriptors utilized in each model [58]. The created models satisfy the criteria $RMSE_{tr}$ and $RMSE_{cv}$. The generated models' high values for the cross-validation parameters Q^2, Q^2_{LMO}, and CCC_{cv} demonstrate their statistical robustness. The low R^2_{Yscr} and Q^2_{Yscr} values for the models show that they were not created by chance. Both models' high values for numerous statistical parameters, such as R^2_{ex}, Q^2_{F1}, Q^2_{F2}, Q^2_{F3}, CCC_{ex}, etc., show that they have a high level of external predictability. The low value of $RMSE_{ex}$ and MAE_{ex} provides additional support for this. Briefly stated, the constructed models satisfy the suggested interrelations and threshold values for a variety of statistical parameters proposed by various scholars [59].

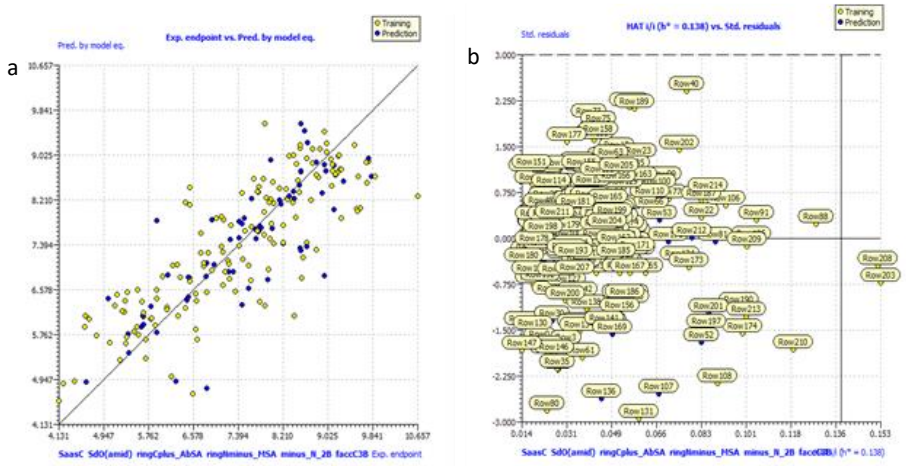

Figure 3. Showing the plot where yellow dots indicate compounds in the training set and blue dots indicate compounds in the prediction set for dpp4 **(a)** Exp. Endpoint vs. Pred. by model eq.; **(b)** Williams plot for assessment of applicability domain, where HAT value is 0.138.

Figure 3(a) represents the scatter plot done with exp. Endpoint vs. Pred. by model eq. This shows that there is a uniform distribution of data points. Yellow dots indicate compounds in the training set, and blue dots indicate compounds in the prediction set [60]. William's plot helps us to identify the applicability domain of the QSAR model. Assessment of the applicability domain is important to identify whether the model can make predictions within chemical space. If there are any chemical compounds that have structural features distinct from

the rest of the compounds in the data set, they will be identified as outliers [61]. HAT value is given here as 0.138, which is the threshold value h*. It is calculated as p K+1/n, where n is the number of compounds in the training set, and K is several descriptors used in the model. Here, compound numbers 203 and 208 are said to be outliers or not fall within the applicability domain, as they are distinct structural features from the rest of the compounds in the data set. Figure 3(b) summarizes William's plot.

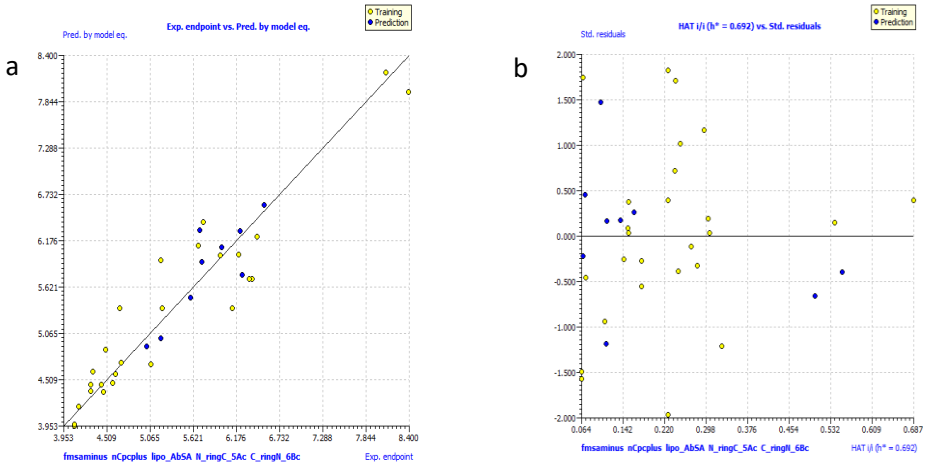

Figure 4. Showing the plot where yellow dots indicate compounds in the training set and blue dots indicate compounds in the prediction set for XO **(a)** Exp. Endpoint vs. Pred. by model eq.; **(b)** Williams plot for assessment of applicability domain, where HAT value is 0.692

These are the scatter plots done with exp. Endpoint vs. Pred. by model eq., summarized in Figure 4 (a), which shows that there is a uniform distribution of data points. Yellow dots indicate compounds in the training set, and blue dots indicate compounds in the prediction set. Williams's plots for Xanthine oxidase are represented in Figure 4 (b), which helps us to identify the applicability domain of the QSAR model. Assessment of the applicability domain is important to identify whether the model can predict within chemical space. Any chemical compounds with structural features distinct from the rest of the data set will be identified as outliers. HAT value is given here as 0.692, which is the threshold value h*. It is calculated as p = K+1/n, where n is the number of compounds in the training set, and K is the number of descriptors used in the model.

3.2. Molecular docking and ADMET.

Molecular docking is a molecular modeling technique used to predict a protein (enzyme) interaction with small molecules (ligands). RMSD < 2.0 A° corresponds to a good docking result. Here we consider the molecules having an RMSD value of zero hence having a good binding affinity [41] ADME and toxicity screening has given three compounds that have high docking scores, more pIC_{50} value, as well as an inactive profile for toxicity such as hepatotoxicity, carcinogenicity, mutagenicity, cytotoxicity, and also following the Lipinski rule, Ghose violation, Veber violation, Egan violation, Muegg violation also having synthetic accessibility, shows in Table 3 [62,63]. ADMET profiling of the top compounds indicated favorable safety and pharmacokinetic properties. hERG prediction indicated low cardiotoxicity risk, while BBB values indicated limited blood–brain barrier penetration, reducing the potential for CNS side effects. These results support the drug-likeness and therapeutic promise of the proposed dual inhibitors.

Table 3. ADME and toxicity screening of novel compounds.

Molecule	Estimated pIC_{50} dpp	Docking DPP4	Estimated pIC_{50} XO	Docking XO	Lipinski #violations	Ghose #violations	Veber #violations	Egan #violations	Muegge #violations	Tox Class	Hepatotoxicity	Carcinogenicity	Immunotoxicity	Mutagenicity	Cytotoxicity	PAINS #alerts	Synthetic Accessibility
Sitagliptine	-	-9.2	-	-	0	0	0	0	0	5	Inactive	Inactive	Inactive	Inactive	inactive	0	3.50
Allopurinol	-	-	-	-4.3	0	3	0	0	1	4	Active	Inactive	Inactive	Inactive	inactive	0	1.76
Molecule 2	6.54	-10.2	6.93	-6.6	0	0	0	0	0	4	inactive	active	inactive	active	inactive	0	2.94
Molecule 4	6.53	-9.3	6.82	-6.8	0	0	0	0	0	4	inactive	active	inactive	active	inactive	0	2.83
Molecule 5	8.26	-10.5	7.70	-7.5	0	0	0	0	0	4	inactive	active	inactive	active	inactive	0	3.17
Molecule 6	9.03	-10.1	6.45	-7.2	0	0	0	0	0	4	inactive	active	inactive	active	inactive	0	3.14
Molecule 8	7.87	-9.9	6.42	-6.5	0	0	0	0	0	4	Inactive	Inactive	Inactive	Inactive	Inactive	0	2.82
Molecule 9	8.01	-9.6	6.74	-6.6	0	0	0	0	0	4	Inactive	Inactive	Inactive	Inactive	Inactive	0	2.86
Molecule 10	8.73	-9.7	6.16	-6.6	0	0	0	0	0	4	Inactive	Inactive	Inactive	Inactive	Inactive	0	3.05
Molecule 11	8.28	-9.8	6.81	-7.2	0	0	0	0	0	4	inactive	active	inactive	active	inactive	0	3.43
Molecule 13	8.09	-9.8	7.88	-7.1	0	0	0	0	0	4	inactive	active	inactive	active	inactive	0	4.43
Molecule 15	6.54	-10.2	6.93	-6.6	0	0	0	0	0	4	inactive	active	inactive	active	inactive	0	2.94
Molecule 17	8.78	-9.8	7.20	-7.5	0	0	0	0	0	4	inactive	active	inactive	active	inactive	0	4
Molecule 18	6.38	-9.3	7.83	-6.9	0	0	0	0	0	4	inactive	active	active	active	inactive	0	2.83
Molecule 19	6.89	-10.3	6.68	-6.8	0	0	0	0	0	4	inactive	active	inactive	active	inactive	0	2.9
Molecule 22	8.02	-8.8	9.36	-6.5	0	0	0	0	0	5	inactive	active	inactive	active	inactive	0	4.05
Molecule 23	8.30	-8.4	11.3	-6.6	0	0	0	0	0	5	inactive	active	inactive	active	inactive	0	4.02
Molecule 24	8.26	-8.6	11.4	-6.6	0	0	0	0	0	5	inactive	active	inactive	active	inactive	0	4.05
Molecule 37	8.33	-9.7	6.28	-7.1	0	0	0	0	0	4	inactive	active	inactive	active	inactive	0	3.1

ADME and toxicity screening were performed for seventeen compounds. Highlighted compounds showing inactive toxicity profiles for hepatotoxicity, carcinogenicity, mutagenicity, cytotoxicity, and synthetic accessibility, with their docking score and pIC_{50} for all 17 compounds

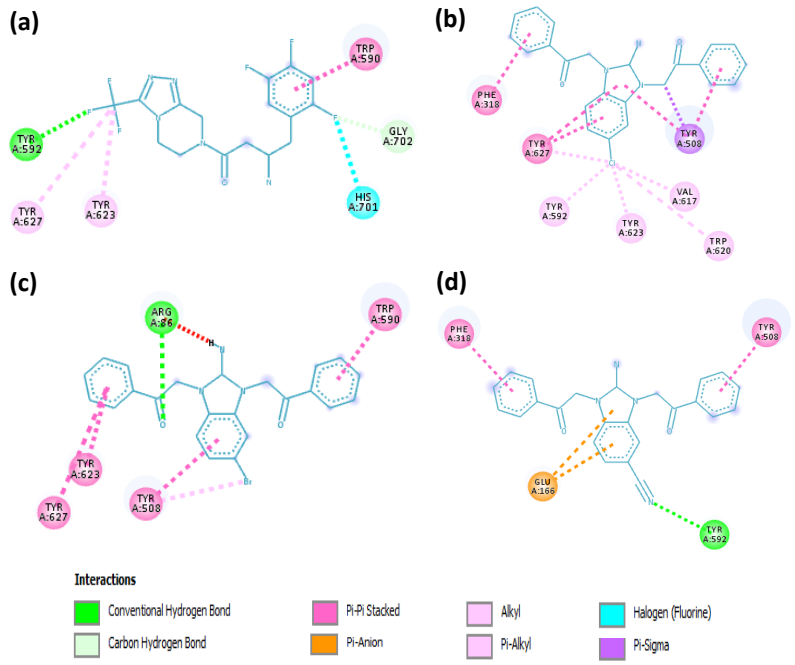

Figure 5. Docking results showing amino acid interaction for the Standard drug of DPP-4 with compounds. **(a)** Standard drug sitagliptin has a pIC_{50} of 7.744 and a docking score is -9.2; **(b)** Compound 8 has a pIC_{50} is 7.876408 and a docking score is -9.9; **(c)** Compound 9 has a pIC_{50} is 8.01 and a docking score is -9.6; **(d)** Compound 10 pIC_{50} is 8.73 and a docking score is -9.7.

The pIC_{50} value of compound no. 08, 09, 10 was found to be more than the standard drug sitagliptin. The docking score is also more than that of the standard drug. Notably, compound 10 demonstrated the highest predicted affinity (docking score: -9.7; pIC_{50}: 8.73),

suggesting potent DPP-4 inhibition. A conventional hydrogen bond is an electrostatic force of attraction between a hydrogen atom, which is covalently bound to a more electronegative atom (which bears a lone pair of electrons). Sitagliptin, a standard DPP-4 drug, forms a conventional hydrogen bond with the Pi-Pi-stacked TYR-592 residue, with an attractive noncovalent interaction between aromatic rings. Sitagliptin also has pi-pi stacked with the TRP-590 residue. Pi-alkyl refers to the interaction between the pi electron of the aromatic group and the electron of the alkyl group. The standard drug for DPP-4 has a pi-alkyl interaction with TYR-623 residue (Figures 5 and 6). Recurrent interactions with TYR-627, TYR-623, TYR-592, and TRP-620 were observed across top-performing compounds and the standard inhibitor. These residues form crucial hydrogen bonds, π-π stacking, and hydrophobic contacts, contributing significantly to the binding affinity and inhibitory potency (Figure 5).

DPP-4 features a classic serine protease catalytic triad of SER-630, ASP-708, HIS-740 amino acids with additional substrate-stabilizing roles for TYR-547, TYR-631, TYR-662, and TYR-666. In this study, the observed ligand interactions with TYR-627, TYR-623, and TRP-620 are adjacent to the catalytic and substrate-binding subsites, highlighting the importance of these contacts in effective DPP-4 inhibition. These residues facilitate ligand anchoring in the enzyme's active site and are vital in rational inhibitor design. These results are similar to previously published literature studies [10].

Docking score of compound no. 08, 09, 10 for Xanthine oxidase is more than the Allopurinol standard drug, with compound 9 displaying the highest predicted activity (pIC50: 6.75; docking score: -6.6) and also shows the interaction with amino acid residue. XO inhibition is primarily mediated by interactions within its molybdenum center-containing active site, where residues including GLN-203, ASN-215, THR-498, and LEU-218 play pivotal roles. Their engagement by the test compounds mirrors key contacts established by allopurinol, substantiating their relevance in the inhibition mechanism (Figure 6).

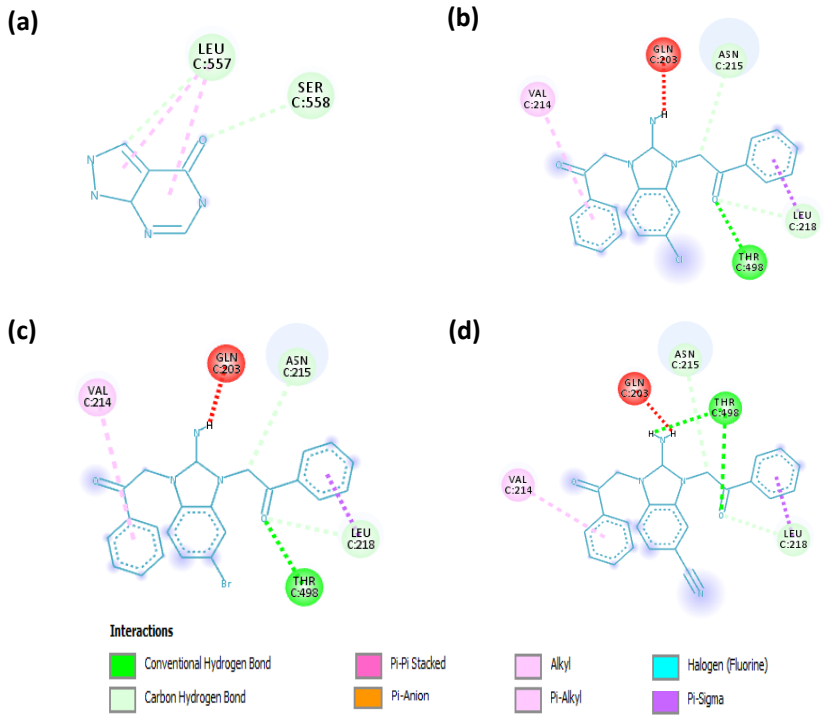

Figure 6. Docking results showing amino acid interaction for the standard drug of XO with compounds. **(a)** Standard drug allopurinol having pIC_{50} 6.699 and docking score -4.3; **(b)** Compound 8 having pIC_{50} 6.420595 and docking score -6.5; **(c)** Compound 9 having pIC_{50} 6.747063, Docking score -6.6; **(d)** Compound 10 having pIC_{50} 6.165173, Docking score -6.6.

Thus, molecular docking identified several novel compounds with favorable binding affinities and interaction patterns at the active sites of DPP-4 and XO. Engagement of key catalytic residues was observed, paralleling the interaction landscapes of established inhibitors.

4. Conclusions

This study identified three promising dual-targeting inhibitors against DPP-4 and XO using structure-based and ligand-based in silico modeling. These compounds 08, 09, and 10 not only demonstrate potent dual inhibitory activity through QSAR modeling and molecular docking but also exhibit favorable drug-likeness and ADMET profiles. These findings underscore the potential of these compounds as next-generation therapeutics for diabetes mellitus and warrant further investigation through preclinical and clinical studies. Additionally, our work highlights the importance of computational modeling in accelerating drug discovery and underscores the significance of structure-activity relationship studies in guiding rational drug design efforts.

Moving forward, our research sets the stage for several avenues of exploration in the field of diabetes mellitus treatment. Firstly, the identified compounds, particularly 08, 09, and 10, merit thorough preclinical evaluation to validate their efficacy and safety profiles. Subsequent clinical trials could ascertain their potential as novel therapeutic agents, offering improved management options for diabetic patients. Furthermore, the QSAR models developed in this study can serve as valuable tools for screening and optimizing new compounds with dual inhibitory activity against DPP-4 and XO enzymes. This opens avenues for the design and synthesis of more potent and selective inhibitors with enhanced therapeutic outcomes and reduced adverse effects. Additionally, the molecular insights gained from our docking studies provide a foundation for further mechanistic investigations and structural modifications to refine drug candidates. Overall, the future endeavors outlined here hold promise for advancing the pharmacotherapy of diabetes mellitus and addressing the unmet medical needs of this prevalent and challenging disease.

Author Contributions

Conceptualization, S. T. and S. S.; Methodology, S. T. and S. S.; Software, S. S.; Validation, S. S. and Z. Z.; Formal analysis, D. C., S. S., and X. X.; Investigation, S. T.; Resources, S. S.; Data curation, S. S.; Writing – original draft, S. T.; Writing – review & editing, S. T. and S. S.; Visualization, S. T. and S. S.; Supervision, S. S. and D. C.; Project administration, S. S.; Funding acquisition, S. S. All authors have read and agreed to the published version of the manuscript.

Institutional Review Board Statement

Not applicable.

Informed Consent Statement

Not applicable.

Data Availability Statement

No new data were created or analyzed in this study. Data sharing is not applicable.

Funding

This research received no specific grant from any funding agency in the public, commercial, or not-for-profit sectors.

Acknowledgments

The authors are thankful to Dr. Satish Chaturvedi, Chairman, LTJSS, Nagpur, for giving moral support. We would like to thank Dr. Vijay Masand, Vidya Bharati College, Amravati, for providing detailed descriptions of the Py-descriptors for model interpretation.

Conflicts of Interest

The authors declare no conflict of interest.

Supplementary materials

Download supplementary materials.

References

1. Moini, J. Chapter 1 - Introduction and History of Diabetes Mellitus. In Epidemiology of Diabetes, Moini, J., Ed.; Elsevier: **2019**; pp. 1-10, https://doi.org/10.1016/B978-0-12-816864-6.00001-8.
2. Raut, N.A.; Dhore, P.W.; Saoji, S.D.; Kokare, D.M. Chapter 9 - Selected Bioactive Natural Products for Diabetes Mellitus. In Studies in Natural Products Chemistry, Atta ur, R., Ed.; Elsevier: **2016**; Volume 48, pp. 287-322, https://doi.org/10.1016/B978-0-444-63602-7.00009-6.
3. Dennery, P.A. Introduction to serial review on the role of oxidative stress in diabetes mellitus. *Free Radic. Biol. Med.* **2006**, *40*, 1-2, https://doi.org/10.1016/j.freeradbiomed.2005.09.003.
4. Duvnjak, L.; Perković, M.N.; Blaslov, K. Dipeptidyl peptidase-4 activity is associated with urine albumin excretion in type 1 diabetes. *J. Diabetes Complic.* **2017**, *31*, 218-222, https://doi.org/10.1016/j.jdiacomp.2016.08.022.
5. Martín-Timón, I.; Sevillano-Collantes, C.; Segura-Galindo, A.; del Cañizo-Gómez, F.J. Type 2 diabetes and cardiovascular disease: have all risk factors the same strength?. *World J. Diabetes* **2014**, *5*, 444, https://doi.org/10.4239/wjd.v5.i4.444.
6. Chang, K.-H.; Chuang, T.-J.; Lyu, R.-K.; Ro, L.-S.; Wu, Y.-R.; Chang, H.-S.; Huang, C.-C.; Kuo, H.-C.; Hsu, W.-C.; Chu, C.-C.; Chen, C.-M. Identification of Gene Networks and Pathways Associated with Guillain-Barré Syndrome. *PLOS ONE* **2012**, *7*, e29506, https://doi.org/10.1371/journal.pone.0029506.
7. Shulman, G.I. Cellular mechanisms of insulin resistance. *J. Clin. Invest.* **2000**, *106*, 171–176, https://doi.org/10.1172/JCI10583.
8. Grunberger, G. Clinical Utility of the Dipeptidyl Peptidase-4 Inhibitor Linagliptin. *Postgrad. Med.* **2013**, *125*, 79–90, https://doi.org/10.3810/pgm.2013.05.2663.
9. Tse, B.C.; Block, B.; Figueroa, H.; Yao, R. Adverse neonatal outcomes associated with pregestational diabetes mellitus in infants born preterm. *Am. J. Obstet. Gynecol. MFM* **2020**, *2*, 100213, https://doi.org/10.1016/j.ajogmf.2020.100213.
10. Zhang, J.; Zhu, Y.-D.; Li, C.-Q.; Fan, Y.-M.; Huo, H.; Sun, C.-G.; Zhou, J.; Sun, L.; Qian, X.-K.; Zou, L.-W. A sensitive fluorescence assay of serum dipeptidyl peptidase IV activity to predict the suitability of its inhibitors in patients with type 2 diabetes mellitus. *J. Pharm. Biomed. Anal.* **2024**, *249*, 116382, https://doi.org/10.1016/j.jpba.2024.116382.
11. Saini, K.; Sharma, S.; Khan, Y. DPP-4 inhibitors for treating T2DM - hype or hope? an analysis based on the current literature. *Front. Mol. Biosci.* **2023**, *10*, 1130625, https://doi.org/10.3389/fmolb.2023.1130625.

12. Cernea, S.; Raz, I. Therapy in the Early Stage: Incretins. *Diabetes Care* **2011**, *34*, S264–S271, https://doi.org/10.2337/dc11-s223.
13. Kanasaki, K.; Shi, S.; Kanasaki, M.; He, J.; Nagai, T.; Nakamura, Y.; Ishigaki, Y.; Kitada, M.; Srivastava, S.P.; Koya, D. Linagliptin-Mediated DPP-4 Inhibition Ameliorates Kidney Fibrosis in Streptozotocin-Induced Diabetic Mice by Inhibiting Endothelial-to-Mesenchymal Transition in a Therapeutic Regimen. *Diabetes* **2014**, *63*, 2120-2131, https://doi.org/10.2337/db13-1029.
14. Mentlein, R. Dipeptidyl-peptidase IV (CD26)-role in the inactivation of regulatory peptides. *Regul. Pept.* **1999**, *85*, 9–24, https://doi.org/10.1016/S0167-0115(99)00089-0.
15. Cooper, M.E.; Perkovic, V.; McGill, J.B.; Groop, P.-H.; Wanner, C.; Rosenstock, J.; Hehnke, U.; Woerle, H.-J.; von Eynatten, M. Kidney Disease End Points in a Pooled Analysis of Individual Patient–Level Data From a Large Clinical Trials Program of the Dipeptidyl Peptidase 4 Inhibitor Linagliptin in Type 2 Diabetes. *Am. J. Kidney Dis.* **2015**, *66*, 441-449, https://doi.org/10.1053/j.ajkd.2015.03.024.
16. Firneisz, G.; Varga, T.; Lengyel, G.; Fehér, J.; Ghyczy, D.; Wichmann, B.; Selmeci, L.; Tulassay, Z.; Rácz, K.; Somogyi, A. Serum Dipeptidyl Peptidase-4 Activity in Insulin Resistant Patients with Non-Alcoholic Fatty Liver Disease: A Novel Liver Disease Biomarker. *PLOS ONE* **2010**, *5*, e12226, https://doi.org/10.1371/journal.pone.0012226.
17. Li, N.; Wang, L.-J.; Jiang, B.; Li, X.-q.; Guo, C.-l.; Guo, S.-j.; Shi, D.-Y. Recent progress of the development of dipeptidyl peptidase-4 inhibitors for the treatment of type 2 diabetes mellitus. *European J. Med. Chem.* **2018**, *151*, 145-157, https://doi.org/10.1016/j.ejmech.2018.03.041.
18. Zhou, Y.; Liu, X.; Li, S.; Liu, C.; Zhang, Y.; Sun, R. Comprehensive profiling of xanthine oxidase inhibitors of *Changbaishan ganoderma* and its treatment of Gout disease. *J. Mol. Struct.* **2025**, *1340*, 142446, https://doi.org/10.1016/j.molstruc.2025.142446.
19. Navarro-Acosta, D.; Coba-Jiménez, L.; León-Sotomayor, W.; Vivas-Reyes, R.; Cubillán, N. Integrative computational approach for hyperuricemia treatment: 3D QSAR, molecular docking and dynamics of flavonoid analogues as xanthine oxidase inhibitors. *J. Mol. Struct.* **2025**, *1322*, 140395, https://doi.org/10.1016/j.molstruc.2024.140395.
20. Taylor, O.M.; Lam, C. The Effect of Dipeptidyl Peptidase-4 Inhibitors on Macrovascular and Microvascular Complications of Diabetes Mellitus: A Systematic Review. *Curr. Ther. Res.* **2020**, *93*, 100596, https://doi.org/10.1016/j.curtheres.2020.100596.
21. Jha, A.; Misra, A.; Gupta, R.; Ghosh, A.; Tyagi, K.; Dutta, K.; Arora, B.; Durani, S. Dipeptidyl peptidase 4 inhibitors linked bullous pemphigoid in patients with type 2 diabetes mellitus: A series of 13 cases. *Diabetes Metab. Syndr.: Clin. Res. Rev.* **2020**, *14*, 213-216, https://doi.org/10.1016/j.dsx.2020.03.001.
22. Tomovic, K.; Ilic, B.S.; Smelcerovic, Z.; Miljkovic, M.; Yancheva, D.; Kojic, M.; Mavrova, A.T.; Kocic, G.; Smelcerovic, A. Benzimidazole-based dual dipeptidyl peptidase-4 and xanthine oxidase inhibitors. *Chem. Biol. Interact.* **2020**, *315*, 108873, https://doi.org/10.1016/j.cbi.2019.108873.
23. Bisht, P.; Gautam, P.; Bhattacharya, A.; Singh, R.; Verma, S.K. Designing of xanthine-based DPP-4 inhibitors: a structure-guided alignment dependent Multifacet 3D-QSAR modeling, and molecular dynamics simulation study. *J. Biomol. Struct. Dyn.* **2025**, *43*, 6971-6995, https://doi.org/10.1080/07391102.2024.2329787.
24. Dey, P.K.; Dutta, R.; Ray, M.; Jakkula, P.; Banerjee, S.; Qureshi, I.A.; Gayen, S.; Amin, S.A. Fragment-based QSAR study to explore the structural requirements of DPP-4 inhibitors: a stepping stone towards better type 2 diabetes mellitus management. *SAR QSAR Environ. Res.* **2024**, *35*, 483-504, https://doi.org/10.1080/1062936X.2024.2366886.
25. Kumar, N.; Kaur, K.; Bedi, P.M.S. Hybridization of molecular docking studies with machine learning based QSAR model for prediction of xanthine oxidase activity. *Comput. Theor. Chem.* **2023**, *1227*, 114262, https://doi.org/10.1016/j.comptc.2023.114262.
26. Wu, Y.; Li, M.; Shen, J.; Pu, X.; Guo, Y. A consensual machine-learning-assisted QSAR model for effective bioactivity prediction of xanthine oxidase inhibitors using molecular fingerprints. *Mol. Divers.* **2024**, *28*, 2033-2048, https://doi.org/10.1007/s11030-023-10649-z.
27. Shah, S.K.; Chaple, D.R.; Masand, V.H.; Jawarkar, R.D.; Chaudhari, S.; Abiramasundari, A.; Zaki, M.E.A.; Al-Hussain, S.A. Multi-Target In-Silico modeling strategies to discover novel angiotensin converting enzyme and neprilysin dual inhibitors. *Sci. Rep.* **2024**, *14*, 15991, https://doi.org/10.1038/s41598-024-66230-7.
28. Maddeboina, K.; Yada, B.; Kumari, S.; McHale, C.; Pal, D.; Durden, D.L. Recent advances in multitarget-directed ligands via *in silico* drug discovery. *Drug Discov. Today* **2024**, *29*, 103904,

https://doi.org/10.1016/j.drudis.2024.103904.
29. Azenabor, A.; Erivona, R.; Adejumo, E.; Ozuruoke, D.; Azenabor, R. Xanthine oxidase activity in type 2 diabetic Nigerians. *Diabetes Metab. Syndr.: Clin. Res. Rev.* **2019**, *13*, 2021-2024, https://doi.org/10.1016/j.dsx.2019.04.022.
30. Ayyappan, P.; Nampoothiri, S.V. Chapter 13 - Bioactive natural products as potent inhibitors of xanthine oxidase. In Studies in Natural Products Chemistry, Atta Ur, R., Ed.; Elsevier: **2020**; Volume 64, pp. 391-416, https://doi.org/10.1016/B978-0-12-817903-1.00013-9.
31. Masand, V.H.; El-Sayed, N.N.E.; Mahajan, D.T.; Mercader, A.G.; Alafeefy, A.M.; Shibi, I.G. QSAR modeling for anti-human African trypanosomiasis activity of substituted 2-Phenylimidazopyridines. *J. Mol. Struct.* **2017**, *1130*, 711-718, https://doi.org/10.1016/j.molstruc.2016.11.012.
32. Kubinyi, H. QSAR and 3D QSAR in drug design Part 1: methodology. *Drug Discov. Today* **1997**, *2*, 457-467, https://doi.org/10.1016/S1359-6446(97)01079-9.
33. Hosoya, H. Topological Index. A Newly Proposed Quantity Characterizing the Topological Nature of Structural Isomers of Saturated Hydrocarbons. *Bull. Chem. Soc. Jpn.* **1971**, *44*, 2332–2339, https://doi.org/10.1246/bcsj.44.2332.
34. Balaban, A.T. Highly discriminating distance-based topological index. *Chem. Phys. Lett.* **1982**, *89*, 399–404, https://doi.org/10.1016/0009-2614(82)80009-2.
35. Jain, N.; Gupta, S.; Sapre, N.; Sapre, N.S. *In silico* de novo design of novel NNRTIs: a bio-molecular modelling approach. *RSC Adv.* **2015**, *5*, 14814-14827, https://doi.org/10.1039/C4RA15478A.
36. Unger, S.H. Molecular Connectivity in Structure–activity Analysis. *J. Pharm. Sci.* **1987**, *76*, 269-270, https://doi.org/10.1002/jps.2600760325.
37. Rahman, S.U.; Ali, H.S.; Jafari, B.; Zaib, S.; Hameed, A.; Al-Kahraman, Y.M.S.A.; Langer, P.; Iqbal, J. Structure-based virtual screening of dipeptidyl peptidase 4 inhibitors and their *in vitro* analysis. *Comput. Biol. Chem.* **2021**, *91*, 107326, https://doi.org/10.1016/j.compbiolchem.2020.107326.
38. Garro Martinez, J.C.; Vega-Hissi, E.G.; Andrada, M.F.; Estrada, M.R. QSAR and 3D-QSAR studies applied to compounds with anticonvulsant activity. *Expert Opin. Drug Discov.* **2015**, *10*, 37-51, https://doi.org/10.1517/17460441.2015.968123.
39. Qiao, K.; Fu, W.; Jiang, Y.; Chen, L.; Li, S.; Ye, Q.; Gui, W. QSAR models for the acute toxicity of 1,2,4-triazole fungicides to zebrafish (*Danio rerio*) embryos. *Environ. Pollut.* **2020**, *265*, 114837, https://doi.org/10.1016/j.envpol.2020.114837.
40. Hadaji, E.; Bouachrine, M.; El Hamdani, H.; Ouammou, A. QSAR and molecular docking study of quinolin derivatives with topoisomerase I inhibitory properties as potential anticancer agents using statistical methods. *Mater. Today: Proc.* **2022**, *51*, 1838-1850, https://doi.org/10.1016/j.matpr.2020.08.032.
41. Xue, L.; Bajorath, J. Molecular Descriptors in Chemoinformatics, Computational Combinatorial Chemistry, and Virtual Screening. *Comb. Chem. High Throughput Screen.* **2000**, *3*, 363-372, https://doi.org/10.2174/1386207003331454.
42. Pablo, R.-F.; Raquel, M.-R.; Francisco, J.P.-P.; Manuel, E.; Cristian, R.M.; Riccardo, C.; Aliuska, D.-S.; Humberto, G.-D. From QSAR models of Drugs to Complex Networks: State-of-Art Review and Introduction of New Markov-Spectral Moments Indices. *Curr. Top. Med. Chem.* **2012**, *12*, 927-960, https://doi.org/10.2174/156802612800166819.
43. Cocchi, M.; De Benedetti, P.G.; Seeber, R.; Tassi, L.; Ulrici, A. Development of Quantitative Structure−Property Relationships Using Calculated Descriptors for the Prediction of the Physicochemical Properties (n_D, ρ, bp, ε, η) of a Series of Organic Solvents. *J. Chem. Inf. Comput. Sci.* **1999**, *39*, 1190-1203, https://doi.org/10.1021/ci9903298.
44. Wiener, H. Structural Determination of Paraffin Boiling Points. *J. Am. Chem. Soc.* **1947**, *69*, 17–20, https://doi.org/10.1021/ja01193a005.
45. Havránková, E.; Peña-Méndez, E.M.; Csöllei, J.; Havel, J. Prediction of biological activity of compounds containing a 1,3,5-triazinyl sulfonamide scaffold by artificial neural networks using simple molecular descriptors. *Bioorg. Chem.* **2021**, *107*, 104565, https://doi.org/10.1016/j.bioorg.2020.104565.
46. Bootsma, A. Rapid Ranking of Heterocycle-Side Chain Stacking Interactions Based on New Molecular Descriptors. *Biophys. J.* **2021**, *120*, 284a, https://doi.org/10.1016/j.bpj.2020.11.1818.
47. Zhong, S.; Hu, J.; Yu, X.; Zhang, H. Molecular image-convolutional neural network (CNN) assisted QSAR models for predicting contaminant reactivity toward OH radicals: Transfer learning, data augmentation and model interpretation. *Chem. Eng. J.* **2021**, *408*, 127998, https://doi.org/10.1016/j.cej.2020.127998.
48. Goudzal, A.; El Aissouq, A.; El Hamdani, H.; Ouammou, A. QSAR modeling, molecular docking studies

and ADMET prediction on a series of phenylaminopyrimidine-(thio) urea derivatives as CK2 inhibitors. *Mater. Today: Proc.* **2022**, *51*, 1851-1862, https://doi.org/10.1016/j.matpr.2020.08.044.
49. Xuan-Yu, M.; Hong-Xing, Z.; Mihaly, M.; Meng, C. Molecular Docking: A Powerful Approach for Structure-Based Drug Discovery. *Curr. Comput. -Aided Drug Des.* **2011**, *7*, 146-157, https://doi.org/10.2174/157340911795677602.
50. Wu, J.; Gao, Y.; Xi, J.; You, X.; Zhang, X.; Zhang, X.; Cao, Y.; Liu, P.; Chen, X.; Luan, Y. A high-throughput microplate toxicity screening platform based on *Caenorhabditis elegans*. *Ecotoxicol. Environ. Saf.* **2022**, *245*, 114089, https://doi.org/10.1016/j.ecoenv.2022.114089.
51. Lee, S.-J.; Baek, S.-K.; Kim, W.; Quah, Y.; Kim, S.-Y.; Jeong, J.-S.; Lee, J.; Yu, W.-J. Reproductive and developmental toxicity screening of bisphenol F by oral gavage in rats. *Regul. Toxicol. Pharmacol.* **2022**, *136*, 105286, https://doi.org/10.1016/j.yrtph.2022.105286.
52. Perin, M.; Dallegrave, A.; da Costa, J.S.; Streit, L.; de Araújo Gomes, A.; Pizzolato, T.M. Identification of the organic compounds in surface water: Suspect screening using liquid chromatography high-resolution mass spectrometry and in silico toxicity evaluation. *Int. J. Mass Spectrom.* **2023**, *484*, 116982, https://doi.org/10.1016/j.ijms.2022.116982.
53. Mombelli, E.; Pandard, P. Evaluation of the OECD QSAR toolbox automatic workflow for the prediction of the acute toxicity of organic chemicals to fathead minnow. *Regul. Toxicol. Pharmacol.* **2021**, *122*, 104893, https://doi.org/10.1016/j.yrtph.2021.104893.
54. Oyewole, R.O.; Oyebamiji, A.K.; Semire, B. Theoretical calculations of molecular descriptors for anticancer activities of 1, 2, 3-triazole-pyrimidine derivatives against gastric cancer cell line (MGC-803): DFT, QSAR and docking approaches. *Heliyon* **2020**, *6*, e03926, https://doi.org/10.1016/j.heliyon.2020.e03926.
55. Rengasamy, K.R.R.; Slavětínská, L.P.; Kulkarni, M.G.; Stirk, W.A.; Van Staden, J. Cuparane sesquiterpenes from *Laurencia natalensis* Kylin as inhibitors of alpha-glucosidase, dipeptidyl peptidase IV and xanthine oxidase. *Algal Res.* **2017**, *25*, 178-183, https://doi.org/10.1016/j.algal.2017.05.008.
56. Shah, S.; Chaple, D.; Masand, V.H.; Zaki, M.E.A.; Al-Hussain, S.A.; Shah, A.; Arora, S.; Jawarkar, R.; Tauqeer, M. *In silico* study to recognize novel angiotensin-converting-enzyme-I inhibitors by 2D-QSAR and constraint-based molecular simulations. *J. Biomol. Struct. Dyn.* **2024**, *42*, 2211-2230, https://doi.org/10.1080/07391102.2023.2203261.
57. Bou-Salah, L.; Benarous, K.; Linani, A.; Bombarda, I.; Yousfi, M. In vitro and in silico inhibition studies of five essential oils on both enzymes human and bovine xanthine oxidase. *Ind. Crops Prod.* **2020**, *143*, 111949, https://doi.org/10.1016/j.indcrop.2019.111949.
58. Allouche, A.-R. Gabedit—A graphical user interface for computational chemistry softwares. *J. Comput. Chem.* **2011**, *32*, 174–182, https://doi.org/10.1002/jcc.21600.
59. Shah, S.K.; Chaple, D.R. 2D-QSAR Modeling of Quinazolinone Derivatives as Angiotensin II Type 1a Receptor Blockers. *Int. J. Quant. Struct.-Prop. Relationships* **2022**, *7*, 1–20, https://doi.org/10.4018/ijqspr.290012.
60. Yuanita, E.; Sudirman; Dharmayani, N.K.T.; Ulfa, M.; Syahri, J. Quantitative structure–activity relationship (QSAR) and molecular docking of xanthone derivatives as anti-tuberculosis agents. *J. Clin. Tuberc. Other Mycobact. Dis.* **2020**, *21*, 100203, https://doi.org/10.1016/j.jctube.2020.100203.
61. Masand, V.H.; Patil, M.K.; El-Sayed, N.N.E.; Zaki, M.E.A.; Almarhoon, Z.; Al-Hussain, S.A. Balanced QSAR analysis to identify the structural requirements of ABBV-075 (Mivebresib) analogues as bromodomain and extraterminal domain (BET) family bromodomain inhibitor. *J. Mol. Struct.* **2021**, *1229*, 129597, https://doi.org/10.1016/j.molstruc.2020.129597.
62. Gedeck, P. Reviews in Computational Chemistry, Volume 10. *J. Mol. Model.* **1997**, *3*, 466, https://doi.org/10.1007/s0089470030466.
63. Garg, R.; Gupta, S.P.; Gao, H.; Babu, M.S.; Debnath, A.K.; Hansch, C. Comparative Quantitative Structure−Activity Relationship Studies on Anti-HIV Drugs. *Chem. Rev.* **1999**, *99*, 3525-3602, https://doi.org/10.1021/cr9703358.

Publisher's Note & Disclaimer